Fast Summation of Functions on the Rotation Group

Ralf Hielscher [*] Jürgen Prestin [†] Antje Vollrath[†, ‡]

Abstract

Computing with functions on the rotation group is a task found in various areas of application. When it comes to approximation kernel based methods are a suitable tool to handle these functions. In this paper we present an algorithm which allows us to evaluate linear combinations of functions on the rotation group as well as an truly fast algorithm to sum up radial functions on the rotation group. These approaches based on nonequispaced FFTs on $SO(3)$ take $\mathcal{O}(M+N)$ arithmetic operations for M and N arbitrarily distributed source and target nodes, respectively. We investigate a selection of radial functions and give explicit theoretical error bounds along with numerical examples on their approximation errors. Moreover we provide an application of our method, namely the kernel density estimation from electron back scattering diffraction (EBSD) data, a problem relevant in texture analysis.

1 Introduction

Functions defined on the rotational group SO(3), i.e., on the group of all rotations of the three dimensional Euclidean space $\mathbb{R}^3$ are of central importance in numerous fields like texture analysis (Bunge, 1982), or protein docking (Kovacs et al., 2003). Recently, fast Fourier techniques have been applied to functions on $\mathrm{SO}(3)$ (cf. Kostelec and Rockmore, 2006, 2008; Potts et al., 2009). From the approximation theory point of view kernel based methods have proved to be a suitable tool for solving a large class of problems on the rotation group, e.g. interpolation, least squares approximation, clustering or principle component analysis (Gutzmer, 1996; Yershova and LaValle, ICRA 2004; Filbir and Schmid, 2008; v.d. Boogaart et al., 2007). Let $\psi \in L^2(\mathrm{SO}(3))$ be a so called *kernel function*, $\mathbf{g}_1, \dots, \mathbf{g}_M \in \mathrm{SO}(3)$ a set of source nodes, and $c_m \in \mathbb{C}$, $m = 1, \dots, M$, complex numbers. Then the evaluation of the sum

$$\sum_{m=1}^{M} c_m \psi(\mathbf{q}_n \mathbf{g}_m^{-1}) = f(\mathbf{q}_n) \tag{1}$$

[*]Chemnitz University of Technology
[†]Institut für Mathematik, Universität zu Lübeck
[‡]Lübeck Graduate School for Computing in Medicine and Life Sciences

at arbitrary target nodes $\mathbf{q}_1, \dots, \mathbf{q}_N \in \mathrm{SO}(3)$ is a central task in all kernel based methods. A real world example where the computation of the sum (1) is required for a huge number of source and target nodes is orientation density estimation from individual orientation measurements, e.g. from EBSD data (cf. Adams et al., 1993). In this case the source nodes are the measured individual orientations, the function ψ is the kernel used for kernel density estimation and the function f represents the estimated orientation density function.

The numerical complexity of a naive algorithm computing the sum (1) at N rotations is $\mathcal{O}(MN)$ which is too large for the applications we have in mind. In this paper we introduce an approximative algorithm for the evaluation of the sum (1) with numerical complexity $\mathcal{O}(M+N)$.

For this aim we use the Fourier partial sum $S_L\psi\colon \mathrm{SO}(3) \to \mathbb{C}$ of the kernel function ψ,

$$S_L\psi = \sum_{\ell=0}^{L} \sum_{k,k'=-\ell}^{\ell} \hat{\psi}_\ell^{k,k'} D_\ell^{k,k'}$$

where $D_\ell^{k,k'}$ are the so called Wigner-D functions on $\mathrm{SO}(3)$ and $\hat{\psi}_\ell^{k,k'}$, $\ell \in \mathbb{N}_0$, $k, k' = -\ell, \dots, \ell$ are the Fourier coefficients of ψ. With this definition the Fourier coefficients of the function f up to the order L can be computed by an adjoint Fourier transform of the coefficients c_m, $m = 1, \dots, M$, followed by a multiplication with the Fourier coefficients $\hat{\psi}_\ell^{k,k'}$, $\ell = 0, \dots, L$, $k, k' = -\ell, \dots, \ell$. Now, evaluating the Fourier partial sum $S_L f$ at the nodes $\mathbf{q}_n$, $n = 1, \dots, N$ is a discrete Fourier transform on $\mathrm{SO}(3)$.

Several techniques have been proposed for the fast evaluation of discrete Fourier transforms on $\mathrm{SO}(3)$. Among them is an approach (cf. Potts et al., 2009) which uses a fast polynomial transform based on three-term recurrence formulae. It converts the $SO(3)$ Fourier sums as a whole into standard Fourier sums on the three-dimensional torus, thus reducing the computational complexity to $\mathcal{O}(L^4 + M)$ steps or even to $\mathcal{O}(L^3 \log^2 L + M)$ if you omit the stabilization scheme. Moreover, a forthcoming paper will use an approach that replaces the fast polynomial transform scheme with a different approximate technique, based on semiseparable matrices. It has a complexity of only $\mathcal{O}(L^3 \log L + M)$ steps.

On the other hand, the multiplication with the Fourier coefficients $\hat{\psi}_\ell^{k,k'}$ has the numerical complexity $\mathcal{O}(L^4)$. Hence, the algorithms proposed in this paper have the total complexity of $\mathcal{O}(M + N + L^4)$. But they have the potential to become algorithms of complexity $\mathcal{O}(M + N + L^3 \log^2 L)$ or even $\mathcal{O}(M + N + L^3 \log L)$ in case of a radial basis function ψ where $\psi(\mathbf{g}) = \psi(\mathbf{q}\mathbf{g}\mathbf{q}^{-1})$ for all $\mathbf{g}, \mathbf{q} \in \mathrm{SO}(3)$.

In addition to the approximation error of the nonequispaced fast SO(3) Fourier transform the accuracy of our algorithm depends on the polynomial cutoff of the kernel function ψ. In our paper we prove error bounds for some of the most important kernel functions like the Abel–Poisson kernel, the de la Vallée Poussin kernel and others and justify the theoretic error bounds by numerical experiments. Finally, we demonstrate the performance of our algorithm at the practical example of the determination of an orientation density function from electron back scattering diffraction (EBSD) data by kernel density estimation.

Fast radial basis function algorithms that utilize fast Fourier techniques to find an Fourier approximation of the function f which then can be evaluated at arbitrary nodes are well established in the Euclidean and the spherical case. They have been discussed in (Potts and Steidl,

2003; Keiner et al., 2006). There they come off well compared to other algorithms like Moving Squares, Thin Plate Splines, partition of unity, or fast multipole (cf. Fasshauer, 2007).

2 Preliminaries

2.1 The Rotation Group

A rotation in $\mathbb{R}^3$ can be identified with an orthogonal matrix $\mathbf{g} \in \mathbb{R}^{3\times 3}$ having determinant $\det(\mathbf{g}) = 1$ making it an orientation-preserving orthogonal transformation. The set of all such matrices $\{\mathbf{g} \in \mathbb{R}^{3\times 3} \mid \det(\mathbf{g}) = 1 \text{ and } \mathbf{g}^{\mathrm{T}} = \mathbf{g}^{-1}\}$ constitutes the special orthogonal group $\mathrm{SO}(3)$. There are various ways to parameterize an element $\mathbf{g} \in \mathrm{SO}(3)$ (see Varshalovich et al., 1988, Sect. 1.4). In this paper we are going to use the well known Euler angles as specified below.

Definition 1. Let $\alpha, \gamma \in [0, 2\pi)$, $\beta \in [0, \pi]$ and let the rotation $\mathbf{g}(\alpha, \beta, \gamma)$ be defined as

$$\mathbf{g}(\alpha, \beta, \gamma) = \mathbf{g}_{\mathrm{Z}}(\alpha)\mathbf{g}_{\mathrm{Y}}(\beta)\mathbf{g}_{\mathrm{Z}}(\gamma)$$

where

$$\mathbf{g}_{\mathrm{Z}}(\varphi) = \begin{pmatrix} \cos\varphi & -\sin\varphi & 0 \\ \sin\varphi & \cos\varphi & 0 \\ 0 & 0 & 1 \end{pmatrix}, \quad \mathbf{g}_{\mathrm{Y}}(\theta) = \begin{pmatrix} \cos\theta & 0 & \sin\theta \\ 0 & 1 & 0 \\ -\sin\theta & 0 & \cos\theta \end{pmatrix}$$

denote rotations about the z- and y-axis, respectively. Then the angles α, β and γ are called *Euler angles* of the rotation $\mathbf{g}(\alpha, \beta, \gamma)$.

For sake of simplicity, we will denote functions $f\colon \mathrm{SO}(3) \to \mathbb{C}$ by $f(\alpha, \beta, \gamma) = f(\mathbf{g}(\alpha, \beta, \gamma))$ when given by their Euler angles.

Instead of splitting a rotation into three consecutive rotations about defined axes one can also describe it by a single axis and an angle denoting how much an object is rotated about the axis. This rotational angle is well defined and defines a metric on the rotational group $\mathrm{SO}(3)$.

Definition 2. The rotational angle of a rotation $\mathbf{g} \in \mathrm{SO}(3)$ is defined as

$$|\mathbf{g}| = \arccos \frac{1}{2}(\operatorname{Tr} \mathbf{g} - 1),$$

where $\operatorname{Tr}\mathbf{g}$ denotes the trace of the matrix $\mathbf{g}$.

Furthermore, we define the distance between two rotations $\mathbf{g}_1, \mathbf{g}_2 \in \mathrm{SO}(3)$ as the rotational angle of the rotation $\mathbf{g}_2\mathbf{g}_1^{-1}$ that transforms $\mathbf{g}_1$ into $\mathbf{g}_2$, i.e.,

$$d(\mathbf{g}_1, \mathbf{g}_2) = \left|\mathbf{g}_2\mathbf{g}_1^{-1}\right|.$$

Remark 3. In terms of Euler angles the rotational angle of a rotation $\mathbf{g} = \mathbf{g}(\alpha, \beta, \gamma) \in \mathrm{SO}(3)$ reads as

$$|\mathbf{g}(\alpha, \beta, \gamma)| = 2 \arccos\left(\cos\frac{\beta}{2}\cos\frac{\alpha+\gamma}{2}\right).$$

2.2 Harmonic Functions on the Rotation Group

Let μ denote the Haar measure on $\mathrm{SO}(3)$. We consider the Hilbert space $L^2(\mathrm{SO}(3))$ with the inner product

$$\begin{aligned}\langle f_1, f_2\rangle_{L^2(\mathrm{SO}(3))} &= \int_{\mathrm{SO}(3)} f_1(\mathbf{g})\overline{f_2(\mathbf{g})}\,\mathrm{d}\mu(\mathbf{g}) \\ &= \int_0^{2\pi}\int_0^{\pi}\int_0^{2\pi} f_1(\alpha,\beta,\gamma)\overline{f_2(\alpha,\beta,\gamma)}\sin\beta\,\mathrm{d}\alpha\,\mathrm{d}\beta\,\mathrm{d}\gamma,\end{aligned}$$

of two functions $f_1, f_2 \in L^2(\mathrm{SO}(3))$.

Related to this inner product we are going to define an orthogonal system in $L^2(\mathrm{SO}(3))$.

Definition 4. Let $\ell \in \mathbb{N}_0$ and $k, k' = -\ell, \ldots, \ell,$. Then the functions

$$D_\ell^{k,k'}(\mathbf{g}(\alpha,\beta,\gamma)) = D_\ell^{k,k'}(\alpha,\beta,\gamma) = \mathrm{e}^{-\mathrm{i}k\alpha}\mathrm{e}^{-\mathrm{i}k'\gamma} d_\ell^{k,k'}(\cos\beta), \tag{2}$$

with

$$d_\ell^{k,k'}(x) = \frac{(-1)^{\ell-k}}{2^\ell}\sqrt{\frac{(\ell+k)!}{(\ell-k')!(\ell+k')!(\ell-k)!}}\sqrt{(1-x)^{k'-k}}\,\frac{\mathrm{d}^{\ell-k}}{\mathrm{d}x^{\ell-k}}\frac{(1+x)^{k'+\ell}}{(1-x)^{k'-\ell}}. \tag{3}$$

are called *Wigner–D functions* or *generalized spherical harmonics* and the functions $d_\ell^{k,k'}$ are called *Wigner-d functions* or *generalized associated Legendre functions*.

The Wigner-D functions can be characterized as the matrix elements of the left regular representation of the group $\mathrm{SO}(3)$ in $L^2(\mathbb{S}^2)$, i.e., they satisfy the representation property

$$D_\ell^{k,k'}(\mathbf{gq}) = \sum_{j=-\ell}^{\ell} D_\ell^{k,j}(\mathbf{g}) D_\ell^{j,k'}(\mathbf{q}). \tag{4}$$

As a consequence, we have by the Peter–Weyl Theorem (cf. Vilenkin, 1968, Sect. 3.3) the orthogonality conditions

$$\int_{\mathrm{SO}(3)} D_{\ell_1}^{k_1k_1'}(\mathbf{g})\overline{D_{\ell_2}^{k_2k_2'}(\mathbf{g})}\,\mathrm{d}\mu(\mathbf{g}) = \frac{8\pi^2}{2\ell+1}\delta_{k_1k_2}\delta_{k_1'k_2'}\delta_{\ell_1\ell_2}. \tag{5}$$

Furthermore, the Wigner-D functions form a complete orthogonal system of $L^2(\mathrm{SO}(3))$, i.e., the harmonic spaces

$$\mathrm{Harm}_\ell(\mathrm{SO}(3)) = \mathrm{span}\left\{D_\ell^{k,k'} \,|\, k,k' = -\ell,\ldots,\ell\right\}$$

spanned by the Wigner-D functions satisfy

$$L^2(\mathrm{SO}(3)) = \mathrm{clos}_{L^2}\bigoplus_{\ell=0}^{\infty}\mathrm{Harm}_\ell(\mathrm{SO}(3)).$$

In particular, the Wigner-D functions $\{D_\ell^{k,k'} \mid \ell \in \mathbb{N}_0, k, k' = -\ell, \dots, \ell\}$ form a orthogonal basis of $L^2(\mathrm{SO}(3))$.

As a consequence a function $f \in L^2(\mathrm{SO}(3))$ has a unique series expansion in terms of the Wigner-D functions

$$f = \sum_{\ell=0}^{\infty} \sum_{k=-\ell}^{\ell} \sum_{k'=-\ell}^{\ell} \widehat{f}_\ell^{k,k'} D_\ell^{k,k'} \tag{6}$$

with Fourier coefficients $\hat{f}_\ell^{k,k'}$ given by the integral

$$\widehat{f}_\ell^{k,k'} \quad = \quad \frac{2\ell+1}{8\pi^2} \langle f, D_\ell^{k,k'} \rangle_{L^2(\mathrm{SO}(3))}. \tag{7}$$

2.3 Nonequispaced Discrete Fourier Transform on the Rotation Group

For any $L \in \mathbb{N}_0$ we consider the space of polynomials of maximum degree L

$$\Pi_L = \bigoplus_{\ell=0}^{L} \mathrm{Harm}_\ell(\mathrm{SO}(3)) \subset L^2(\mathrm{SO}(3))$$

and define the index set

$$\mathcal{J}_L = \{(\ell, k, k') \mid \ell = 0, \dots, L; k, k' = -\ell, \dots, \ell\} \tag{8}$$

consisting of all admissible indices (ℓ, k, k') corresponding to polynomials in Π_L. The function spaces Π_L have the dimension

$$\dim(\Pi_L) = |\mathcal{J}_L| = \sum_{\ell=0}^{L} (2\ell+1)^2 = \frac{1}{3}(L+1)(2L+1)(2L+3).$$

Definition 5. Let $G_M = (\mathbf{g}_1, \dots, \mathbf{g}_M)$, $\mathbf{g}_m \in \mathrm{SO}(3)$ be a finite sequence of rotations. Then the operator

$$\mathbf{D}_{L,G_M} \colon \mathbb{C}^{\mathcal{J}_L} \to \mathbb{C}^M, \quad \left[\mathbf{D}_{L,G_M} \hat{\mathbf{f}}\right]_m = f(\mathbf{g}_m) = \sum_{\ell=0}^{L} \sum_{k=-\ell}^{\ell} \sum_{k'=-\ell}^{\ell} \hat{f}_\ell^{k,k'} D_\ell^{k,k'}(\mathbf{g}_m), \quad m = 1, \dots, M, \tag{9}$$

that evaluates a polynomial $f \in \Pi_L$ at the nodes $\mathbf{g}_1, \dots, \mathbf{g}_M$ given its Fourier coefficients $\hat{\mathbf{f}} = (\hat{f}_\ell^{k,k'})_{(\ell,k,k') \in \mathcal{J}_L}$ is called *nonequispaced discrete* $\mathrm{SO}(3)$ *Fourier transform (NDSOFT).*

In matrix-vector notation, the NDSOFT reads

$$\mathbf{f} = \mathbf{D}_{L,G_M} \hat{\mathbf{f}}$$

with the vectors $\mathbf{f} = (f(\mathbf{g}_m))_{m=1,\dots,M}$, $\hat{\mathbf{f}} = (\hat{f}_\ell^{k,k'})_{(\ell,k,k') \in \mathcal{J}_L}$ and the Fourier matrix

$$\mathbf{D}_{L,G_M} = \left(D_\ell^{k,k'}(\mathbf{g}_m) \right)_{m=1,\dots,M;\, (\ell,k,k') \in \mathcal{J}_L}. \tag{10}$$

The application of the adjoint operator $\mathbf{D}_{L,G_M}^{\mathrm{H}} \colon \mathbb{C}^M \to \mathbb{C}^{\mathcal{J}_L}$ is called *adjoint NDSOFT*. Let $\mathbf{W} = \operatorname{diag}(w_m)_{m=1,\dots,M}$. Then

$$\tilde{\mathbf{f}} = \mathbf{D}_{L,G_M}^{\mathrm{H}} \, \mathbf{W} \, \mathbf{f}$$

may be rewritten as

$$\tilde{f}_\ell^{k,k'} = \sum_{m=1}^{M} w_m \, f(\mathbf{g}_m) \, \overline{\tilde{D}_\ell^{k,k'}(\mathbf{g}_m)} \qquad (\ell,k,k') \in \mathcal{J}_L. \tag{11}$$

which for suitable weights w_m, $m = 1,\dots,M$, can be interpreted as a quadrature rule for the calculation of the Fourier coefficients of f, i.e., $\tilde{\mathbf{f}} \approx \hat{\mathbf{f}}$.

If implemented directly, the computation of (9) and (11) takes $\mathcal{O}(ML^3)$ operations. However, as we already mentioned in the introduction there are fast algorithms that perform this computation. In our numerical study, we used the approximate algorithm called the *nonequispaced fast* $\mathrm{SO}(3)$ *Fourier transform (NFSOFT)* described in (Potts et al., 2009). It computes the sums (9) and (11) in $\mathcal{O}(M+L^4)$ steps. Hence the input nodes only contribute additively to the complexity.

2.4 Radial Functions on the Rotation Group

Using the distance measure from Definition 2 we define radial functions on $\mathrm{SO}(3)$.

Definition 6. We call a function $f \colon \mathrm{SO}(3) \to \mathbb{C}$ a *radial function* with center $\mathbf{g}_0 \in \mathrm{SO}(3)$ if it depends only on the rotational distance to $\mathbf{g}_0 \in \mathrm{SO}(3)$, i.e., $f(\mathbf{g}_1) = f(\mathbf{g}_2)$ for all $\mathbf{g}_1, \mathbf{g}_2 \in \mathrm{SO}(3)$ with $d(\mathbf{g}_1, \mathbf{g}_0) = d(\mathbf{g}_2, \mathbf{g}_0)$.

The class of square integrable radial functions on $\mathrm{SO}(3)$ may also be characterized by the following property of their Fourier coefficients (cf. Hielscher, 2007).

Lemma 7. *Let $f \in L^2(\mathrm{SO}(3))$. Then f is a radial function with center $\mathbf{g}_0 \in \mathrm{SO}(3)$ if and only if there is a sequence of coefficients $(\hat{f}_\ell) \in \ell^2(\mathbb{N}_0)$ such that*

$$\hat{f}_\ell^{k,k'} = \hat{f}_\ell D_\ell^{k,k'}(\mathbf{g}_0), \quad \ell \in \mathbb{N}_0, \, k,k' = -\ell,\dots,\ell.$$

In particular,

$$f(\mathbf{g}) \sim \sum_{\ell=0}^{\infty} \hat{f}_\ell \sum_{k,k'=-\ell}^{\ell} D_\ell^{k,k'}(\mathbf{g}_0) D_\ell^{k,k'}(\mathbf{g}) \sim \sum_{\ell=0}^{\infty} \hat{f}_\ell \, \mathcal{U}_{2\ell}\Big(\cos \frac{d(\mathbf{g}_0,\mathbf{g})}{2}\Big),$$

where

$$\mathcal{U}_\ell(\cos\omega) = \frac{\sin(\ell+1)\omega}{\sin\omega}, \quad \ell \in \mathbb{N}_0, \, \omega \in (0,\pi)$$

denote the Chebyshev polynomials of second kind with $\mathcal{U}_\ell(1) = \ell+1$ and $\mathcal{U}_\ell(-1) = (-1)^\ell(\ell+1)$.

Let us conclude with some radial functions on $\mathrm{SO}(3)$ on which we will elaborate further in our numerical tests.

The Generating Function The generating function of the Chebyshev polynomials of second kind is given by (cf. Askey, 1975, Sec. 7)

$$\sum_{\ell=0}^{\infty} \kappa^\ell \mathcal{U}_\ell(t) = \frac{1}{1 - 2\kappa t + \kappa^2}, \quad t \in [-1, 1], \kappa \in (0, 1). \tag{12}$$

We fit into the framework of Lemma 7 by symmetrizing the generating function using $\mathcal{U}_\ell(t) = (-1)^\ell \mathcal{U}_\ell(-t)$. For any $\kappa \in (0, 1)$ we define a radial basis function $\psi \colon \mathrm{SO}(3) \to \mathbb{R}$ by

$$\psi(\mathbf{g}) = \sum_{\ell=0}^{\infty} \kappa^{2\ell} \mathcal{U}_{2\ell}\left(\cos\frac{|\mathbf{g}|}{2}\right) = \frac{\frac{1}{2}}{1 - 2\kappa\cos\frac{|\mathbf{g}|}{2} + \kappa^2} + \frac{\frac{1}{2}}{1 + 2\kappa\cos\frac{|\mathbf{g}|}{2} + \kappa^2}, \quad \mathbf{g} \in \mathrm{SO}(3).$$

In particular, ψ defines a positive, monotonously decreasing radial function on $\mathrm{SO}(3)$. The parameter κ determines the sharpness of the peak of ψ and we have $\psi(\mathrm{Id}) \to \infty$ as $\kappa \to 1$.

The Abel–Poisson Kernel By differentiating (12) with respect to κ a second summation formula for the Chebyshev polynomials is obtained

$$\sum_{\ell=0}^{\infty} (2\ell + 1)\kappa^\ell \mathcal{U}_\ell(t) = \frac{1 - \kappa^2}{(1 - 2\kappa t + \kappa^2)^2}, \quad t \in [-1, 1], \kappa \in (0, 1). \tag{13}$$

Again, by symmetrization we derive the well known *Abel–Poisson kernel* on $\mathrm{SO}(3)$ (Matthies et al., 1987, Sec. 17)

$$\begin{aligned}\psi(\mathbf{g}) &= \sum_{\ell=0}^{\infty} (2\ell + 1)\kappa^{2\ell} \mathcal{U}_{2\ell}\left(\cos\frac{|\mathbf{g}|}{2}\right) \\ &= \frac{1}{2}\left(\frac{1 - \kappa^2}{(1 - 2\kappa\cos\frac{|\mathbf{g}|}{2} + \kappa^2)^2} + \frac{1 - \kappa^2}{(1 + 2\kappa\cos\frac{|\mathbf{g}|}{2} + \kappa^2)^2}\right), \quad \mathbf{g} \in \mathrm{SO}(3).\end{aligned}$$

The de la Vallée Poussin Kernel A radial function combining such nice features as non-negativity, monotonicity and finite Fourier-Chebyshev expansion is the *de la Vallée Poussin kernel*. For any $\kappa \in \mathbb{N}$ it is defined as

$$\psi(\mathbf{g}) = \frac{(2\kappa + 1)2^{2\kappa}}{\binom{2\kappa+1}{\kappa}} \cos^{2\kappa}\frac{|\mathbf{g}|}{2} = \binom{2k + 1}{k}^{-1} \sum_{\ell=0}^{\kappa} (2\ell + 1)\binom{2\kappa + 1}{\kappa - \ell} \mathcal{U}_{2\ell}\left(\cos\frac{|\mathbf{g}|}{2}\right).$$

For proofs of the above properties as well as of the summing formula we refer to (Berens and Xu, 1991).

The von Mises–Fisher Kernel For any $\kappa > 0$ the *von Mises–Fisher kernel* on $\mathrm{SO}(3)$ is defined as (cf. Hielscher, 2007)

$$\psi(\mathbf{g}) = \sum_{\ell=0}^{\infty} \frac{\mathcal{I}_\ell(\kappa) - \mathcal{I}_{\ell+1}(\kappa)}{\mathcal{I}_0(\kappa) - \mathcal{I}_1(\kappa)} \mathcal{U}_{2\ell}\left(\cos\frac{|\mathbf{g}|}{2}\right) = \frac{1}{\mathcal{I}_0(\kappa) - \mathcal{I}_1(\kappa)} e^{\kappa\cos|\mathbf{g}|}, \quad \mathbf{g} \in \mathrm{SO}(3), \tag{14}$$

where $\mathcal{I}_n$, $n \in \mathbb{N}_0$ denote the modified Bessel functions of first kind

$$\mathcal{I}_n(\kappa) = \frac{1}{\pi}\int_0^\pi e^{\kappa\cos\omega}\cos n\omega \,\mathrm{d}\omega.$$

The Gauss-Weierstrass Kernel For $\kappa > 0$ the Gauss-Weierstrass kernel on $\mathrm{SO}(3)$ is defined by its Fourier series

$$\psi(\mathbf{g}) = \sum_{\ell=0}^{\infty} (2\ell+1) e^{-\ell(\ell+1)\kappa} \mathcal{U}_{2\ell}\left(\cos\frac{|\mathbf{g}|}{2}\right).$$

Non-negativity and monotonicity of this kernel function are a consequence of the Bochner theorem (cf Bochner, 1954).

3 Fast Summation

Let $G_M = (\mathbf{g}_1, \dots, \mathbf{g}_M)$, $\mathbf{g}_m \in \mathrm{SO}(3)$ and $Q_N = (\mathbf{q}_1, \dots, \mathbf{q}_M)$, $\mathbf{q}_n \in \mathrm{SO}(3)$ be a list of rotations, $\psi\colon \mathrm{SO}(3) \to \mathbb{C}$ a pointwise given function, and $\mathbf{c} = (c_1, \dots, c_M) \in \mathbb{C}^M$ a coefficient vector. We are concerned with evaluating the sum

$$f(\mathbf{q}_n) = \sum_{m=1}^{M} c_m \psi(\mathbf{q}_n \mathbf{g}_m^{-1}), \quad n = 1, \dots, N, \tag{15}$$

for all rotations $\mathbf{q}_n \in Q_N$. We will call the rotations $\mathbf{g}_m \in G_M$ source nodes and the rotations $\mathbf{q}_n \in Q_N$ target nodes.

Let us first assume that the function $\psi\colon \mathrm{SO}(3) \to \mathbb{C}$ in the sum (15) is a radial function. In this case our approach is almost identical to the fast summation algorithm for radial functions on the sphere (Keiner et al., 2006). We approximate the function ψ by its truncated Fourier series expansion (cf. Lemma 7)

$$S_L\psi(\mathbf{q}\mathbf{g}^{-1}) = \sum_{\ell=0}^{L} \sum_{k,k'=-\ell}^{\ell} \hat{\psi}(\ell) D_\ell^{k,k'}(\mathbf{q}) \overline{D_\ell^{k,k'}(\mathbf{g})}, \quad \mathbf{g}, \mathbf{q} \in \mathrm{SO}(3), \tag{16}$$

with a fixed cut off degree $L \in \mathbb{N}_0$ and substitute it into the sum (1). This leads to a separation of the source nodes $\mathbf{g}_m$, $m = 1, \dots, M$, and the target nodes $\mathbf{q}_n$, $n = 1, \dots, N$,

$$f(\mathbf{q}_n) \approx S_L f(\mathbf{q}_n) = \sum_{\ell=0}^{L} \sum_{k,k'=-\ell}^{\ell} \hat{\psi}(\ell) \left(\sum_{m=1}^{M} c_m \overline{D_\ell^{k,k'}(\mathbf{g}_m)} \right) D_\ell^{k,k'}(\mathbf{q}_n). \tag{17}$$

Based on this representation our fast summation algorithm splits into three steps:

1. The calculation of the innermost sum which is an adjoint nonequispaced Fourier transform that can be approximately computed for the M source nodes $\mathbf{g}_m$ using a NFSOFT with numerical complexity up to $\mathcal{O}(L^4 + M)$.

2. The multiplication with the Fourier coefficients $\hat{\psi}(\ell)$ in $\mathcal{O}(L^3)$ steps.

3. The computation of the outer sums which is essentially a nonequispaced discrete $\mathrm{SO}(3)$ Fourier transform evaluated at the target nodes $\mathbf{q}_n$, $n = 1, \ldots, N$, and can be computed approximately by an NFSOFT with numerical complexity up to $\mathcal{O}(L^4 + N)$.

Expressing the original summation problem (15) as the matrix vector product

$$\mathbf{f} = \mathbf{\Psi}\mathbf{c}$$

with

$$\mathbf{f} = (f(\mathbf{q}_n))_{n=1,\ldots,N} \in \mathbb{C}^N,\ \mathbf{\Psi} \in \mathbb{C}^{N\times M},\ \Psi_{nm} = \psi(\mathbf{q}_n\mathbf{g}_m^{-1}) \text{ and } \mathbf{c} = (c_1, \ldots, c_M) \in \mathbb{C}^M$$

the fast summation algorithm corresponds to a rank $|\mathcal{J}_L|$ approximation $\mathbf{\Psi}_L \in \mathbb{C}^{N\times M}$ of the matrix $\mathbf{\Psi}$. In fact, we compute

$$\mathbf{f}_L = \mathbf{\Psi}_L\mathbf{c},$$

with

$$\mathbf{f}_L = (S_L f(\mathbf{q}_n))_{n=1,\ldots,N} \in \mathbb{C}^N, \text{ and } \mathbf{\Psi}_L \in \mathbb{C}^{N\times M}, \quad [\mathbf{\Psi}_L]_{nm} = S_L\psi(\mathbf{q}_n\mathbf{g}_m^{-1}).$$

In particular the matrix $\mathbf{\Psi}_L$ factorizes into

$$\mathbf{\Psi}_L = \mathbf{D}_{L,Q_N}\hat{\mathbf{\Psi}}_L\mathbf{D}_{L,G_M}^H,$$

where $\mathbf{D}_{L,Q_N}$, $\mathbf{D}_{L,G_M}$ are the Fourier matrices as defined in (10) and $\hat{\mathbf{\Psi}}_L \in \mathbb{C}^{|\mathcal{J}_L|\times|\mathcal{J}_L|}$ is given by

$$\hat{\mathbf{\Psi}}_L = \mathrm{diag}(\hat{\boldsymbol{\psi}}_L),\ [\hat{\boldsymbol{\psi}}_L]_{\ell,k,k'} = \hat{\psi}(\ell).$$

The proposed method is summarized in Algorithm 1.

In the case that the function ψ is not radial its truncated Fourier series expansion may be written using the representation property (4) of the Wigner–D functions as

$$S_L\psi(\mathbf{q}\mathbf{g}^{-1}) = \sum_{\ell=0}^{L}\sum_{k,k'=-\ell}^{\ell}\hat{\psi}(\ell,k,k')\sum_{j=-\ell}^{\ell}D_\ell^{kj}(\mathbf{q})\overline{D_\ell^{k'j}(\mathbf{g})}, \quad \mathbf{g},\mathbf{q} \in \mathrm{SO}(3).$$

Substitution in (15) and rearranging of the sums again yields a separation of source and target nodes

$$f(\mathbf{q}) \approx S_L f(\mathbf{q}) = \sum_{\ell=0}^{L}\sum_{k,k'=-\ell}^{\ell}D_\ell^{k,k'}(\mathbf{q})\sum_{j=-\ell}^{\ell}\hat{\psi}(\ell,k,j)\sum_{m=1}^{M}c_m\overline{D_\ell^{k'j}(\mathbf{g}_m)},$$

Algorithm 1: Fast summation of radial functions on $\mathrm{SO}(3)$.

Input : $M \in \mathbb{N},\ N \in \mathbb{N}$
$\mathbf{g}_m \in \mathrm{SO}(3),\ m = 1, \ldots, M$ /* source nodes */
$\mathbf{c} \in \mathbb{C}^M$ /* coefficients */
$\mathbf{q}_n \in \mathrm{SO}(3),\ n = 1, \ldots, N$ /* target nodes */
$L \in \mathbb{N}_0$ /* cut off parameter */
$\hat{\psi}(\ell) \in \mathbb{C}, \ell = 0, \ldots, L$ /* Fourier coefficients */

Compute $\hat{\mathbf{c}} = \mathbf{D}_{L,G_M}^H \mathbf{c}$ by an adjoint NFSOFT.
Compute $\hat{\mathbf{f}}_L = \hat{\mathbf{\Psi}}_L \hat{\mathbf{c}}$.
Compute $\mathbf{f}_L = \mathbf{D}_{L,Q_N} \hat{\mathbf{f}}_L$ by an NFSOFT.

Output : $\mathbf{f}_L \in \mathbb{C}^N$ /* approximating $\mathbf{f} = \mathbf{\Psi c}$ */
Complexity: $\mathcal{O}(M + N + L^4 L)$

where the innermost sum is an adjoint Fourier transform and the outer most sum is a direct Fourier transform. In contrast to the radial case Step 2 now consists of $L + 1$ matrix - matrix multiplications

$$\hat{\mathbf{f}}_\ell = \hat{\boldsymbol{\psi}}_\ell \hat{\mathbf{c}}_\ell, \quad \ell = 0, \ldots, L, \tag{18}$$

where matrices of Fourier coefficients $\hat{\mathbf{f}}_\ell, \hat{\boldsymbol{\psi}}_\ell, \hat{\mathbf{c}}_\ell \in \mathbb{C}^{(2\ell+1)\times(2\ell+1)}$ are defined as

$$[\hat{\boldsymbol{\psi}}_\ell]_{k,k'} = \hat{\psi}(\ell, k, k'), \quad [\hat{\mathbf{c}}_\ell]_{k,k'} = [\mathbf{D}_{L,G_M} \mathbf{c}]_{l,k,k'} \text{ and } [\hat{\mathbf{f}}_\ell]_{k,k'} = \hat{f}_{\ell,k,k'}, \quad k, k' = -\ell, \ldots, \ell.$$

Together, these matrix multiplications have the numerical complexity $\mathcal{O}(L^4)$. This results in the overall complexity $\mathcal{O}(L^4 + N + M)$ of our fast summation algorithm, which is described in Algorithm 2.

Algorithm 2: Fast summation on $\mathrm{SO}(3)$.

Input : $M \in \mathbb{N},\ N \in \mathbb{N}$
$\mathbf{g}_m \in \mathrm{SO}(3),\ m = 1, \ldots, M$ /* source nodes */
$\mathbf{c} \in \mathbb{C}^M$ /* coefficients */
$\mathbf{q}_n \in \mathrm{SO}(3),\ n = 1, \ldots, N$ /* target nodes */
$L \in \mathbb{N}_0$ /* cut off parameter */
$\hat{\psi}(\ell, k, k') \in \mathbb{C}$ /* Fourier coefficients */
$l = 0, \ldots, L,\ k, k' = -\ell, \ldots, \ell$

Compute $\hat{\mathbf{c}} = \mathbf{D}_{L,G_M}^H \mathbf{c}$ by an adjoint NFSOFT.
Compute $\hat{\mathbf{f}}_\ell = \hat{\boldsymbol{\psi}}_\ell \hat{\mathbf{c}}_\ell$, $\ell = 0, \ldots, L$.
Compute $\mathbf{f}_L = \mathbf{D}_{L,Q_N} \hat{\mathbf{f}}$ by an NFSOFT

Output : $\mathbf{f}_L \in \mathbb{C}^N$ /* approximating $\mathbf{f} = \mathbf{\Psi c}$ */
Complexity: $\mathcal{O}(M + N + L^4)$

4 Error Estimates

Next we discuss the error introduced by the approximation of $\mathbf{\Psi}$ by $\mathbf{\Psi}_L$. Obviously, this error depends on the decay rate of the Fourier coefficients $\hat{\psi}$.

Lemma 8. *Let $\psi \in L^\infty(\mathrm{SO}(3))$ be a radial function and let $f \in L^\infty(\mathrm{SO}(3))$ and $S_L f \in \Pi_L$ be defined as in* (15) *and* (16)*. Then we have the error estimate*

$$\|f - S_L f\|_\infty \leq \|\mathbf{c}\|_1 \sum_{l>L} (2\ell+1) \left|\hat{\psi}(\ell)\right|. \tag{19}$$

For a not necessarily radial function $\psi \in L^\infty(\mathrm{SO}(3))$ the error is bounded by

$$\|f - S_L f\|_\infty \leq \|\mathbf{c}\|_1 \sum_{\ell>L} \sqrt{2\ell+1}\, \|\hat{\boldsymbol{\psi}}_\ell\|_F, \tag{20}$$

where $\|\hat{\boldsymbol{\psi}}_\ell\|_F$ denotes the Frobenius norm of the matrix $\hat{\boldsymbol{\psi}}_\ell \in \mathbb{C}^{(2\ell+1)\times(2\ell+1)}$.

Proof. The first assertion follows from

$$\|f - S_L f\|_\infty \leq \sum_{m=1}^{M} |c_m| \max_{\mathbf{q}\in\mathrm{SO}(3)} \left| \sum_{\ell>L} \left|\hat{\psi}(\ell)\right| \mathcal{U}_{2\ell}\left(\cos\frac{|\mathbf{q}\mathbf{g}_m^{-1}|}{2}\right)\right|.$$

For the second assertion we rearrange the values of the Wigner-D functions at $\mathbf{g} \in \mathrm{SO}(3)$ as matrices $\mathbf{D}_\ell(\mathbf{g}) \in \mathbb{C}^{(2\ell+1)\times(2\ell+1)}$ with

$$[\mathbf{D}_\ell(\mathbf{g})]_{k,k'} = D_\ell^{k,k'}(\mathbf{g}).$$

Hence, we can write

$$\begin{aligned}
\|f - S_L f\|_\infty &\leq \sum_{m=1}^{M} |c_m| \max_{\mathbf{q}\in\mathrm{SO}(3)} \left| \sum_{\ell>L} \sum_{k,k'=-\ell}^{\ell} \hat{\psi}_\ell^{k,k'} D_\ell^{k,k'}(\mathbf{q}) \right| \\
&= \|\mathbf{c}\|_1 \max_{\mathbf{q}\in\mathrm{SO}(3)} \left| \sum_{\ell>L} \operatorname{Tr} \hat{\boldsymbol{\psi}}_\ell^H \mathbf{D}_\ell(\mathbf{q}) \right|.
\end{aligned}$$

Applying the Cauchy Schwarz inequality to the Frobenius inner product we obtain

$$\begin{aligned}
\|f - S_L f\|_\infty &\leq \|\mathbf{c}\|_1 \max_{\mathbf{q}\in\mathrm{SO}(3)} \sum_{\ell>L} \|\hat{\boldsymbol{\psi}}_\ell\|_F \left(\operatorname{Tr} \mathbf{D}_\ell(\mathbf{q}) \mathbf{D}_\ell^H(\mathbf{q})\right)^{1/2} \\
&= \|\mathbf{c}\|_1 \max_{\mathbf{q}\in\mathrm{SO}(3)} \sum_{\ell>L} \|\hat{\boldsymbol{\psi}}_\ell\|_F \mathcal{U}_{2\ell}(1)^{1/2} \\
&= \|\mathbf{c}\|_1 \sum_{\ell>L} \sqrt{2\ell+1}\, \|\hat{\boldsymbol{\psi}}_\ell\|_F.
\end{aligned}$$

□

Analogously to (Keiner et al., 2006) one obtains immediately the following approximation error between the matrices $\mathbf{\Psi}$ and $\mathbf{\Psi}_L$ with respect to the p–matrix norm.

Corollary 9. *For a radial function $\psi \in L^\infty(\mathrm{SO}(3))$ and $1 \leq p \leq \infty$ we have the following condition on the p–matrix norm*

$$\|\mathbf{\Psi} - \mathbf{\Psi}_L\|_p \leq M^{1-\frac{1}{p}} N^{\frac{1}{p}} \sum_{\ell>L} (2\ell+1) \left|\hat{\psi}(\ell)\right|.$$

For a general $\psi \in L^\infty(\mathrm{SO}(3))$ one has

$$\|\mathbf{\Psi} - \mathbf{\Psi}_L\|_p \leq M^{1-\frac{1}{p}} N^{\frac{1}{p}} \sum_{\ell>L} \|\hat{\boldsymbol{\psi}}_\ell\|_F.$$

Let us finish this section by giving error estimates for $\frac{\|f-S_L f\|_\infty}{\|\mathbf{c}\|_1}$ if ψ is one of the particular kernels defined in Section 2.4 by considering the sum

$$\sum_{\ell=L+1}^{\infty} (2\ell+1) \left|\hat{\psi}(\ell)\right|.$$

First we obtain an error estimate for the radial function derived from the generating function of the Chebyshev polynomials by

$$\begin{aligned} \sum_{\ell=L+1}^{\infty} (2\ell+1)\kappa^{2\ell} &= \kappa^{2L+2}\left(\frac{2L}{1-\kappa^2} + \frac{3-\kappa^2}{(1-\kappa^2)^2}\right) \\ &= \mathcal{O}(L\kappa^{2L}) \qquad \text{for fixed } 0<\kappa<1,\ L\to\infty. \end{aligned}$$

Analogously, for the Abel–Poisson kernel we have

$$\begin{aligned} \sum_{\ell=L+1}^{\infty} (2\ell+1)^2\kappa^{2\ell} &= \kappa^{2L+2}\left(\frac{4L(L+1)}{1-\kappa^2} + \frac{8L+9+\kappa^4-2\kappa^2}{(1-\kappa^2)^3}\right) \\ &= \mathcal{O}(L^2\kappa^{2L}) \qquad \text{for fixed } 0<\kappa<1,\ L\to\infty. \end{aligned} \tag{21}$$

For the Gauss-Weierstrass kernel we have

$$\begin{aligned} \sum_{\ell=L+1}^{\infty} (2\ell+1)^2 \mathrm{e}^{-\ell(\ell+1)\kappa} &< \sum_{\ell=L+1}^{\infty} (2\ell+1)^2 \mathrm{e}^{-(L+1)(\ell+1)\kappa} \\ &= \mathrm{e}^{-(L+1)^2\kappa}\left(\frac{4L(L+1)}{\mathrm{e}^{(L+1)\kappa}-1} + \frac{(8L+9)\mathrm{e}^{2(L+1)\kappa}+1-2\mathrm{e}^{(L+1)\kappa}}{(\mathrm{e}^{(L+1)\kappa}-1)^3}\right) \\ &= \mathcal{O}(L^2\mathrm{e}^{-(L+1)(L+2)\kappa}) \qquad \text{for fixed } \kappa>0,\ L\to\infty. \end{aligned}$$

For the von Mises-Fisher kernel we use orthogonality of the cosine system. Under the condition that we chose $\ell > \kappa + 2$, the resulting sum can be approximated by the error estimate in

the Leibniz criterion. This yields

$$\begin{aligned}
&\left|\sum_{r=0}^{\infty}\frac{\kappa^r}{\pi r!}\int_0^{\pi}\cos^r\omega(\cos\ell\omega-\cos(\ell+1)\omega)\,\mathrm{d}\omega\right| \\
&= \left|\sum_{r=\ell}^{\infty}\frac{\kappa^r}{\pi r!}\int_0^{\pi}\cos^r\omega(\cos\ell\omega-\cos(\ell+1)\omega)\,\mathrm{d}\omega\right| \\
&= \left|\sum_{r=\ell}^{\infty}\frac{\kappa^r}{\pi r!}\left(\frac{(-1)^r2^{-\ell}\pi^{\frac{3}{2}}\cos\frac{\pi}{2}(\ell+r)\Gamma(1+r)}{\Gamma(\frac{1+\ell-r}{2})\Gamma(1-\ell+r)\Gamma(\frac{2+\ell+r}{2})}-\frac{(-1)^r2^{-\ell}\pi^{\frac{3}{2}}\cos\frac{\pi}{2}(1+\ell+r)\Gamma(1+r)}{2\Gamma(\frac{2+\ell-r}{2})\Gamma(-\ell+r)\Gamma(\frac{3+\ell+r}{2})}\right)\right| \\
&< \frac{\kappa^\ell}{2^\ell\ell!}.
\end{aligned}$$

Hence, we first estimate

$$\begin{aligned}
&\sum_{\ell=L+1}^{\infty}(2\ell+1)\left|\frac{\mathcal{I}_\ell(\kappa)-\mathcal{I}_{\ell+1}(\kappa)}{\mathcal{I}_0(\kappa)-\mathcal{I}_1(\kappa)}\right| \\
&\quad= \frac{1}{\mathcal{I}_0(\kappa)-\mathcal{I}_1(\kappa)}\sum_{\ell=L+1}^{\infty}(2\ell+1)\left|\sum_{r=0}^{\infty}\frac{\kappa^r}{\pi r!}\int_0^{\pi}\cos^r\omega(\cos\ell\omega-\cos(\ell+1)\omega)\,\mathrm{d}\omega\right| \\
&\quad< \frac{1}{\mathcal{I}_0(\kappa)-\mathcal{I}_1(\kappa)}\sum_{\ell=L+1}^{\infty}\frac{(2\ell+1)\kappa^\ell}{2^\ell\ell!}.
\end{aligned}$$

This sum can be estimated by two geometric series. Thus one obtains

$$\begin{aligned}
&\frac{1}{\mathcal{I}_0(\kappa)-\mathcal{I}_1(\kappa)}\sum_{\ell=L+1}^{\infty}\frac{(2\ell+1)\kappa^\ell}{2^\ell\ell!} \\
&\quad< \frac{1}{\mathcal{I}_0(\kappa)-\mathcal{I}_1(\kappa)}\left(\frac{\kappa^{L+1}}{2^L L!}\sum_{s=0}^{\infty}\left(\frac{\kappa}{2(L+1)}\right)^s+\frac{\kappa^{L+1}}{2^{L+1}(L+1)!}\sum_{s=0}^{\infty}\left(\frac{\kappa}{2(L+2)}\right)^s\right) \\
&\quad= \frac{\kappa^{L+1}}{\mathcal{I}_0(\kappa)-\mathcal{I}_1(\kappa)}\left(\frac{(L+1)}{2^{L-1}L!(2(L+1)-\kappa)}+\frac{(L+2)}{2^{L+1}(L+1)!(2(L+2)-\kappa)}\right) \\
&\quad= \mathcal{O}\left(\frac{\kappa^L}{L!}\right) \qquad \text{for fixed } \kappa>0,\ L\to\infty.
\end{aligned}$$

Since the de la Vallée Poussin kernel has a finite Fourier expansion the approximation error becomes exactly zero when choosing the cutoff degree $L=\kappa$. However, for very large κ truncating the Fourier expansion at a cutoff degree $L<\kappa$ might be desirable. Rewriting the approximation error for the de la Vallée Poussin kernel in terms of binomial coefficients

$$\sum_{\ell=L}^{\kappa}\frac{(2\ell+1)^2\kappa!(\kappa+1)!}{(\kappa-\ell)!(\kappa+\ell+1)!}=\frac{4}{\binom{2\kappa+1}{\kappa}}\sum_{\ell=0}^{\kappa-L}(\kappa+\frac{1}{2}-\ell)^2\binom{2\kappa+1}{\ell}$$

we observe that it is the truncated variance sum of the binomial distribution $B_n(\ell) = 2^{-2n}\binom{n}{\ell}$. Since the centered and scaled binomial distribution converges to the normal distribution

$$N_{\mu,\sigma}(x) = \frac{1}{\sqrt{2\pi}\sigma} e^{-\frac{1}{2}\frac{(x-\mu)^2}{\sigma^2}}$$

with mean $\mu = 0$ and standard deviation $\sigma = 1$ we have for the approximation error the asymptotic estimate for $\lambda \to \infty$ and $L = \lambda\sqrt{\kappa + \frac{1}{2}} \in \mathbb{N}$

$$\begin{aligned} \frac{\|f - S_L f\|_\infty}{\|\mathbf{c}\|_1} &= \frac{\binom{2\kappa+1}{\kappa}}{(2\kappa+1)2^{2\kappa}} \sum_{\ell=L}^{\kappa} \frac{(2\ell+1)^2 \kappa!(\kappa+1)!}{(\kappa-\ell)!(\kappa+\ell+1)!} \\ &= \frac{4}{2\kappa+1} 2^{-2\kappa} \sum_{\ell=0}^{\kappa-L} (\kappa + \frac{1}{2} - \ell)^2 \binom{2\kappa+1}{\ell} \to 4\int_\lambda^\infty \ell^2 \,\mathrm{d}N_{0,1}(\ell). \end{aligned} \tag{22}$$

Next we want to show that there is an upper bound for the approximation error that does not depend on κ and decays exponentially in λ. Therefore, we first need the following estimate of the binomial distribution by the Gaussian distribution.

Lemma 10. *Let $n, \ell \in \mathbb{N}$ and $\varepsilon \in \{0, \frac{1}{2}\}$ such that $\frac{n}{2} + \varepsilon \in \mathbb{N}$. Then*

$$B_n(\frac{n}{2} + \varepsilon + \ell) \le \frac{B_n(\frac{n}{2}+\varepsilon)}{N_{0,\frac{\sqrt{n+1}}{2}}(\varepsilon)} N_{0,\frac{\sqrt{n+1}}{2}}(\ell + \varepsilon) \le C N_{0,\frac{\sqrt{n+1}}{2}}(\ell + \varepsilon),$$

where the constant $C > 0$ does not depend on n and ℓ.

Proof. Using $\frac{1-x}{1+x} \le e^{-2x}$ for $x \in [0,1]$ we obtain

$$\frac{B_n(\frac{n}{2}+\varepsilon+\ell+1)}{B_n(\frac{n}{2}+\varepsilon+\ell)} = \frac{\binom{n}{\frac{n}{2}+\varepsilon+\ell+1}}{\binom{n}{\frac{n}{2}+\ell+\varepsilon}} = \frac{n - (\frac{n}{2}+\varepsilon+\ell)}{\frac{n}{2}+\varepsilon+\ell+1} = \frac{1 - \frac{2(\varepsilon+\ell)+1}{n+1}}{1 + \frac{2(\varepsilon+\ell)+1}{n+1}} \le e^{-2\frac{2(\varepsilon+\ell)+1}{n+1}} = \frac{e^{-\frac{1}{2}\frac{(\varepsilon+\ell+1)^2}{(n+1)/4}}}{e^{-\frac{1}{2}\frac{(\varepsilon+\ell)^2}{(n+1)/4}}}.$$

This gives the left inequality. The right inequality follows by Stirling's formula. □

Lemma 11. *Let $L = \lambda\sqrt{\kappa + \frac{1}{2}} \in \mathbb{N}$. Then the approximation error $\frac{\|f - S_L f\|_\infty}{\|\mathbf{c}\|_1}$ for the de la Vallée Poussin kernel is uniformly bounded for all $\kappa \in \mathbb{N}$ and decays exponentially with $\lambda \to \infty$.*

Proof. Using Lemma 10 with (22) we obtain for $\kappa \in \mathbb{N}$,

$$\begin{aligned} \frac{\|f - S_L f\|_\infty}{\|\mathbf{c}\|_1} &= \frac{1}{\kappa+\frac{1}{2}} \sum_{\ell=0}^{\kappa-L} (\kappa + \tfrac{1}{2} - \ell)^2 B_{2\kappa+1}(\ell) \\ &\le \frac{1}{\kappa+\frac{1}{2}} \sum_{\ell=0}^{\kappa-L} (\kappa + \tfrac{1}{2} - \ell)^2 C N_{(0,\sqrt{\kappa+\frac{1}{2}}/2)}(\kappa + \frac{1}{2} - \ell) \\ &\le \frac{C}{(\kappa+\frac{1}{2})^{3/2}} \sum_{\ell=0}^{\kappa-L} (\kappa + \tfrac{1}{2} - \ell)^2 e^{-\frac{1}{2}\frac{(\kappa+\frac{1}{2}-\ell)^2}{(\kappa+\frac{1}{2})/2}} \\ &\le \frac{C}{(\kappa+\frac{1}{2})^{3/2}} \int_{-\infty}^{-\lambda\sqrt{\kappa+\frac{1}{2}}} l^2 e^{-\frac{1}{2}\frac{\ell^2}{(\kappa+\frac{1}{2})/2}} \,\mathrm{d}\ell \le C \int_{-\infty}^{-\lambda} (\ell+1)^2 e^{-\frac{1}{8}(\ell-1)^2} \,\mathrm{d}\ell. \end{aligned}$$

Since the last term decays exponentially in λ the lemma is shown.

□

5 Numerical Tests and Applications

5.1 Numerical Tests

We now present some numerical examples to demonstrate performance and accuracy of the fast kernel summation as described in our algorithms. The algorithms were implemented in C and tested on a 3.00 GHz Intel Xenon™ computer with 12 GB main memory, SuSe-Linux (64 bit), using double precision arithmetic. In addition we used the FFTW 3.0.1 (Frigo and Johnson, 2009) and NFFT 3.0.2 (Keiner et al., 2009a,b) libraries as well as the NFSOFT (Potts et al., 2009). Whenever involved we used the NFFT with oversampling factor $\rho = 2$, precomputed Kaiser-Bessel functions and NFFT-intern cut-off parameter $m = 10$.
In our numerical experiments we focus on two main aspects of our algorithm. Firstly, we examine the approximation error between the directly computed sum (15) and the fast computed one from (17). Secondly, we compare the time requirements of our algorithm to the time requirements of the direct summation.

Approximation Errors According to Lemma 8 we choose the quotient

$$E_\infty = \frac{||\mathbf{f} - \mathbf{f}_L||_\infty}{||\mathbf{c}||_1} \tag{23}$$

as a measure for the approximation error we are interested in. Here, the vector $\mathbf{f} = (f(q_n))_{n=1,\dots,N} \in \mathbb{C}^N$ contains the directly computed values of f at the target nodes $q_n \in \mathrm{SO}(3)$, while we compute $\mathbf{f}_L = (S_L f(q_n))_{n=1,\dots,N} \in \mathbb{C}^N$ by using Algorithm 1. The target nodes $q(\alpha, \beta, \gamma)$ as well as the source nodes $g(\alpha, \beta, \gamma)$ were chosen pseudo-randomly from the cuboid $[0, 2\pi) \times [0, \pi] \times [0, 2\pi)$. Furthermore the vector $\mathbf{c} = (c_m)_{m=1,\dots,M} \in \mathbb{C}^M$ contains M-many pseudo-random coefficients from the complex square $\left[-\frac{1}{2}, \frac{1}{2}\right] \times \left[-\frac{\mathrm{i}}{2}, \frac{\mathrm{i}}{2}\right]$.

While the error E_∞ does not depend on the number of target nodes N we see a slight dependancy on the number of source nodes M, i.e., the error becomes smaller for growing M. This is due to the choice of our error measure, in particular, to the denominator $||\mathbf{c}||_1$. This however does not contradict the results of Lemma 8 which states that there is an upper bound independent of the number of source nodes M. Figure 1 confirms this.

Since we are interested in the maximum error we have chosen for our next experiments the number N of targets nodes sufficiently large to ensure that the discrete error E_∞ is almost equal to the true error in (20), i.e., $\|\mathbf{f} - \mathbf{f}_L\|_\infty \approx \|f - S_L f\|_\infty$ for large N. On account of Figure 1 we choose $M = N = 10^5$ for the next tests. Apart from the number of source and target nodes we examined how the approximation error E_∞ depends on the cut off degree L, and on the function ψ.

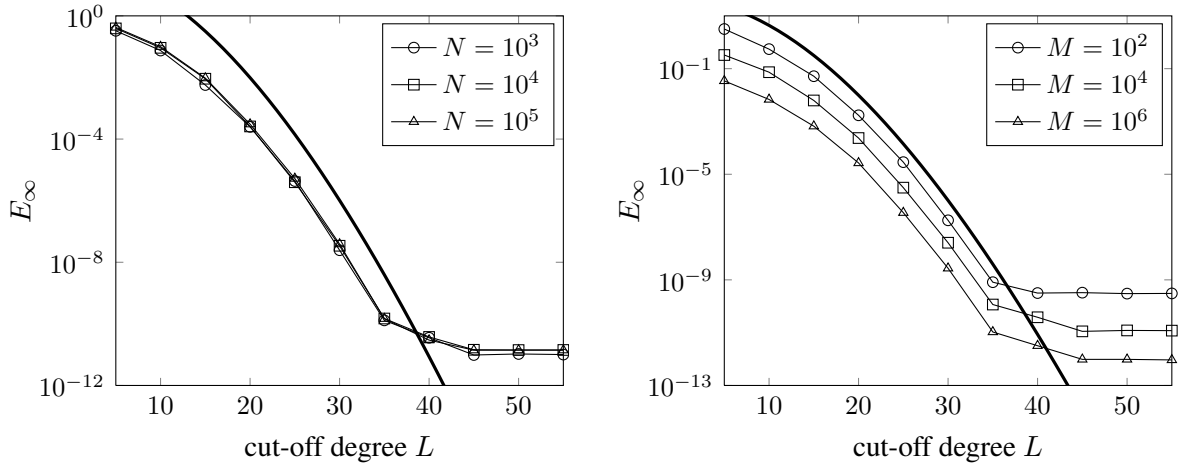

Figure 1: This figure shows the accuracy as a function of the cut-off degree L where we used the van Mises Fisher kernel with $\kappa = 25$. In the left graph we fixed the number of source nodes $M = 10^3$ and plotted the accuracy for different choices of N target nodes. The right graph shows the contrary setting where we fixed the number of target nodes $N = 10^3$ and plotted the accuracy for various numbers M of source nodes. The solid, bold line in both graphs shows the theoretical error bound from equation (21).

The Abel–Poisson Kernel At first we examine the Abel–Poisson kernel. Figure 1 already showed some measured errors as well as the theoretical error bound for this kernel. In addition to that, we now plot the error E_∞ as a function of the cut off degree L for different choices of the parameter κ which controls the localization of the kernel. To give an idea about this localization property we also plot the kernels chosen in each of the summations.

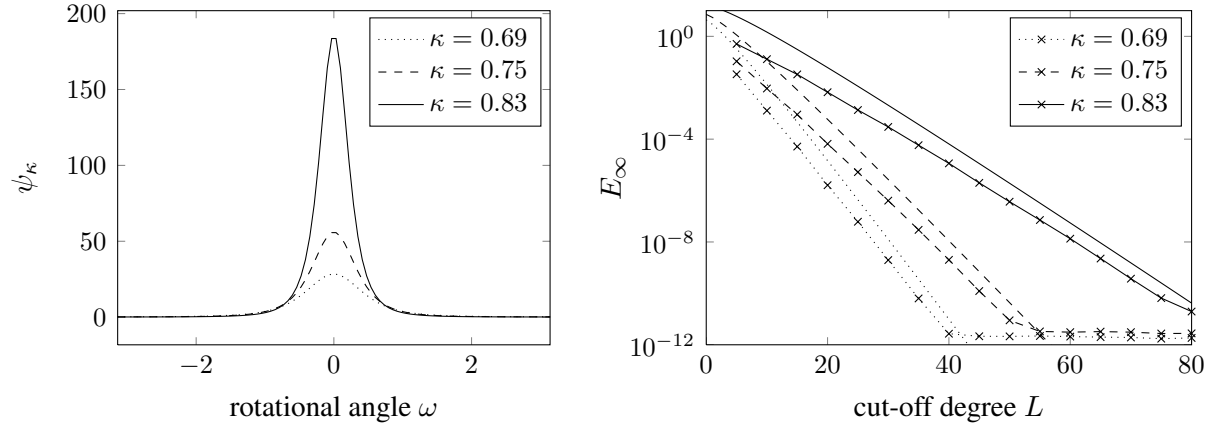

Figure 2: The left part of the figure shows the Abel–Poisson kernel ψ_κ for different parameters κ. The right graphs give the approximation error (23) of our fast algorithm in dependency of the cut-off degree L of the Fourier expansion (17). The tickles graphs show the theoretical bounds (21) whereas the markers give the numerical errors.

The von Mises–Fisher Kernel For the von Mises-Fisher kernel we again show the error E_∞ as a function of the cut off degree L for different choices of the parameter κ and compare it to the theoretical error bound found in (22). Figure 3 shows that the numerical error curves are decreasing much faster and have a sharper bend, than the ones for the Abel–Poisson kernel. This is due to the nicer localization properties of the von Mises-Fisher kernel.

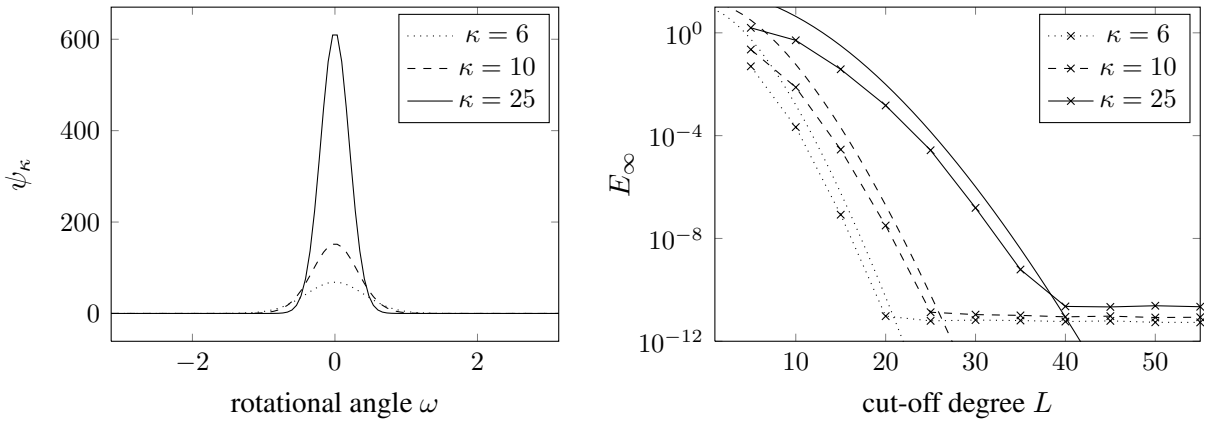

Figure 3: The left part of the figure shows the Mises Fisher kernel ψ_κ for different parameters κ. The right graphs give the approximation error (23) of our fast algorithm in dependency of the cut-off degree L of the Fourier expansion (17). The tickles graphs show the theoretical bounds (22) whereas the markers give the numerical errors.

The de la Vallée Poussin Kernel The third type of kernel used in our experiments is the de la Vallée Poussin kernel. A fact that distinguishes it from the previously considered kernel is its error bound which is independent from the localization parameter κ as seen in Equation (22).

Time requirements After analyzing the accuracy of our algorithm we like to examine its time requirements. We compare the direct algorithm (15) to the fast summation (17) using NFSOFT to perform Algorithm 1.

We like to point out that we call our algorithm a "fast" RBF algorithm because we reduced the total complexity from $\mathcal{O}(MN)$ to $\mathcal{O}(M + N + L^3 \log L)$ where M and N are the number of source and target nodes and L^3 is the dimension of the approximation space. Note that the latter contributes additively in our algorithm, which mean that our algorithm will perform faster then the direct algorithm as long as the dimension of the approximation space is less then the product of the number of source and target nodes.

As in our first experiment we consider the van Mises Fisher kernel with $\kappa = 25$ and set the number of source and target nodes to be equal $M = N$. As it can be seen in Figure 1 our test function f in terms of harmonic functions requires a polynomial degree of 40 in order to get a reasonable approximation with an error in the order of magnitude of 10^{-11}. On the rotation group the function space of polynomials up to degree $L = 40$ has the dimension $\frac{1}{3}(L + 1)(2L +$

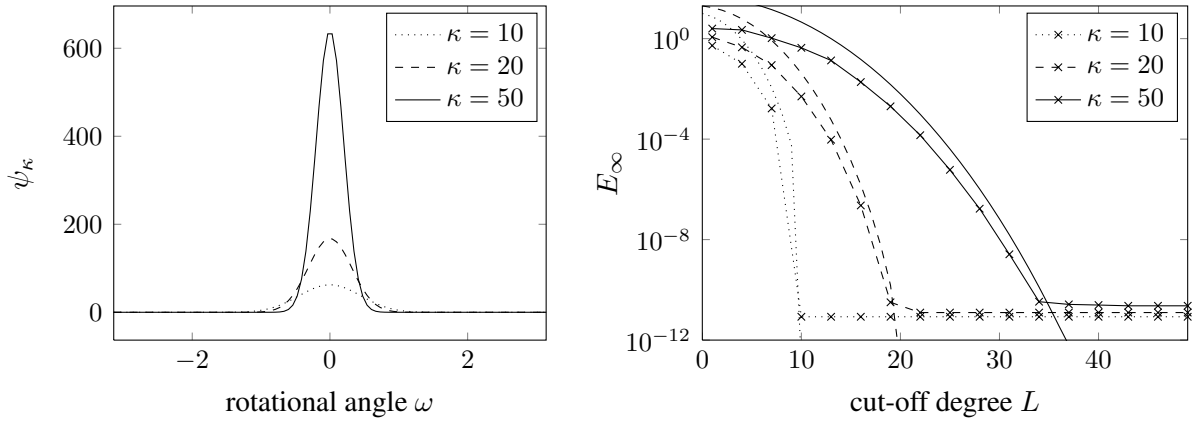

Figure 4: The left part of the figure shows the de la Vallée Poussin kernel ψ_κ for different parameters κ. The right graphs give the approximation error (23) of our fast algorithm in dependency of the cut-off degree L of the Fourier expansion (17). The tickles graphs show the theoretical bounds (22) whereas the markers give the numerical errors.

$1)(2L + 3) = 91\,881$. Indeed, for $M = N = 10^5$ source and target nodes no strong over or undersampling of the function f can be observed (see Figure 5). In the case a larger error is acceptable the polynomial degree of the approximation can be chosen correspondingly smaller (cf. Figure 1). In Figure 6 we compare the performance of our algorithm for different polynomial degrees and increasing number of source and target nodes. Due to the lack of implementations of other algorithms like Moving Squares, Thin Plate Splines, partition of unity, or fast multipole to the rotational group $SO(3)$ the direct algorithm is the only algorithm to whom we can compare our algorithm.

As expected our fast algorithm outperforms the direct summation. Moreover, we can verify that the time requirements of the direct algorithm are increasing as $\mathcal{O}(MN)$ while the fast summation algorithm only shows growth of $\mathcal{O}(M + N)$. This example also shows another phenomenon. The time performance of our fast algorithm is dominated by the cut off degree L of $S_L f$ as long as the number of nodes does not exceed $M \geq L^3$. Thus we see an almost constant time effort for $M < L^3$ while afterwards the time is controlled by the number of nodes as the graphs for all three cut-off degrees approach each other.

5.2 Kernel Density Estimation from EBSD Data

In quantitative texture analysis one is concerned with polycrystalline specimen and investigates the relationship between the orientation of the crystals and the macroscopic properties of the specimen. The orientation of a single crystal is described by an equivalence class of rotations $[\mathbf{g}] \in \mathrm{SO}(3)/S$ where $S \subset \mathrm{SO}(3)$ is the symmetry group of the crystal. The distribution of crystal orientations within the specimen is modeled by the so called *orientation density function* (ODF) $f\colon \mathrm{SO}(3)/S \to \mathbb{R}$ which is defined as the relative frequency of crystal orientations by volume.

Experimentally the ODF of an specimen can be determined by measuring single crystal ori-

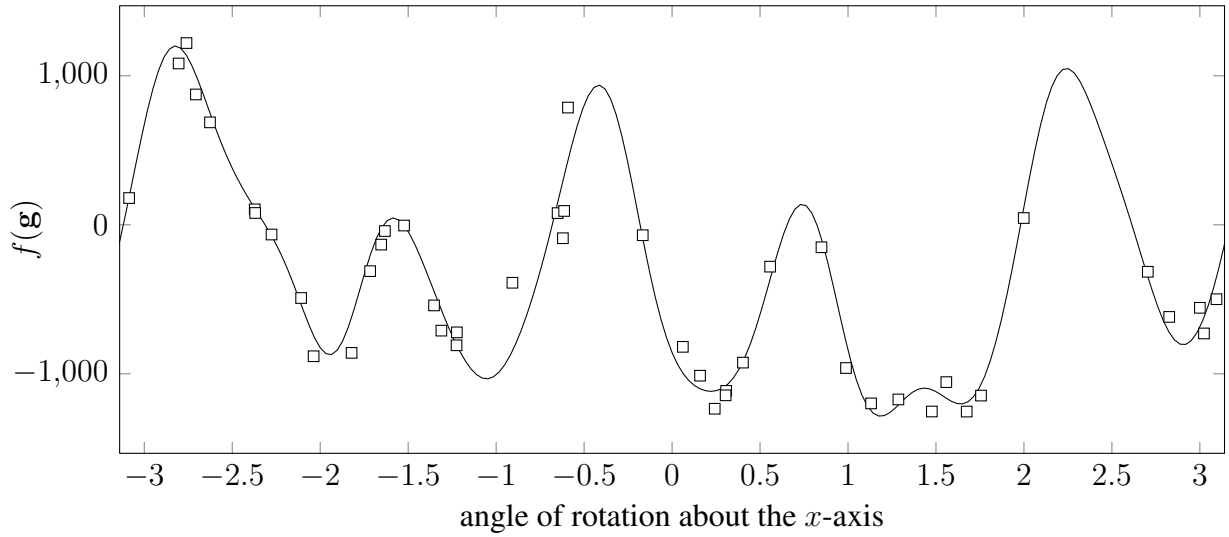

Figure 5: This figure shows the function f plotted along all rotations about the x-axis in dependency of the angle of rotation. The squares represent the function value at all of those of the $N = 10^5$ randomly chosen target nodes that are at distance of at most 2.5 degree from a rotation about the x-axis. The deviation of the squares from the graph of the function f indicates the variation of the function f orthogonal to plotting path.

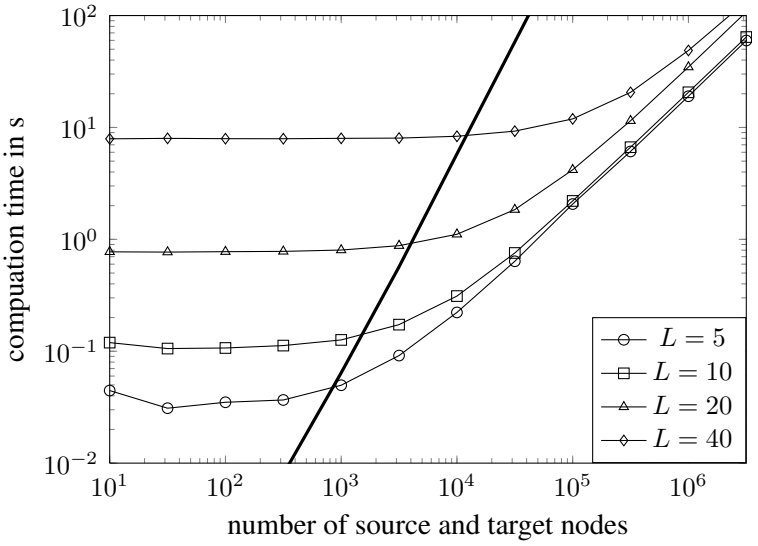

Figure 6: This figure shows the time needed to compute the sums (1) depending on the number of source and target nodes $M = N$. We compare the direct computation via equation (14) (solid, bold line) to the fast summation (17) using the NFSOFT with different cut-off degrees L.

entations $G_M = ([\mathbf{g}_1], \dots, [\mathbf{g}_M])$ with $[\mathbf{g}_m] \in \mathrm{SO}(3)/S$ via electron back scattering diffraction (EBSD) (cf. Adams et al., 1993). These orientations can be interpreted as a random sample of the unknown ODF.

Let $\psi\colon \mathrm{SO}(3) \to \mathbb{R}$ be a nonnegative, radial function with integral one. Then the *kernel density estimator* of the unknown ODF $f\colon \mathrm{SO}(3)/S \to \mathbb{R}$ given the random sample $G_M \subset \mathrm{SO}(3)/S$ is defined as (cf. van den Boogaart, 2001)

$$\tilde{f}_{G_M}([\mathbf{q}]) = \frac{1}{M\,|S|} \sum_{m=1}^{M} \sum_{\mathbf{s}\in S} \psi(\mathbf{q}\mathbf{s}\mathbf{g}_m^{-1}), \tag{24}$$

where $\mathbf{q} \in [\mathbf{q}]$ and $\mathbf{g}_m \in [\mathbf{g}_m]$ are arbitrary representatives of the corresponding equivalent classes.

Since (24) is of the form (15) with coefficients $c_{m,\mathbf{s}} = \frac{1}{M|S|}$, $m = 1, \dots, M$, $\mathbf{s} \in S$, we are in the setting of Algorithm 1. Fixing a cutoff degree $L \in \mathbb{N}$ the numerical complexity for the evaluation of (24) in $N \in \mathbb{N}$ arbitrary orientations $[\mathbf{q}_n] \in \mathrm{SO}(3)/S$ is $\mathcal{O}(M\,|S| + N + L^4)$.

Rewriting (24) as

$$\tilde{f}_{G_M}([\mathbf{q}]) = \frac{1}{M} \sum_{m=1}^{M} \psi_S(\mathbf{q}^{-1}\mathbf{g}_m) \qquad \text{with} \qquad \psi_S(\mathbf{q}) = \frac{1}{|S|} \sum_{\mathbf{s}\in S} \psi(\mathbf{q}\mathbf{s}) \tag{25}$$

we obtain the setting of Algorithm 2 since ψ_S is not radially symmetric. The numerical complexity $\mathcal{O}(M + N + L^4)$ of this approach compares favorable to the previous one if the random sample $\mathbf{G}_M$ contains more then $\frac{L^4}{|S|}$ orientations.

In order to demonstrate the performance of our algorithms we use an EBSD data set of a Ferit specimen measured by I. Lischewski at the department of physical metallurgy and metal physics, Aachen, Germany, which consists of 124.000 single orientations. A plot of the raw EBSD data is shown in Figure 7a. Therefore, the Euler angles representation was used to assign to each orientation an RGB–color, which is plotted in a the map.

We apply kernel density estimation with the radially function ψ defined as the de la Vallée Poussin kernel with parameter $\kappa = 23$ and evaluate the function $\tilde{f}_{G_M}$ at $N = 10^4$ nodes and compare three different ways of calculating the sum (24). First we use a naive implementation that evaluates the functions $\psi(\mathbf{g}_m(\mathbf{q}\mathbf{s})^{-1})$ directly at the given nodes. Second we apply Algorithm 1 for the radially symmetric function ψ to the symmetrized set of nodes SG_M; and third we apply Algorithm 2 to the symmetrized kernel ψ and the set of nodes G_M. Since, the de la Vallée Poussin kernel is a polynomial all the computations are exact.

The corresponding runtimes of the algorithms were $18000s$ for the direct evaluation of the sums, $520s$ for Algorithm 1, and $22s$ for Algorithm 2. This shows the practical relevance of the presented algorithms. A plot of the ODF $\tilde{f}_{G_M}$ is shown in Figure 7b.

References

Adams BL, Wright SI, Kunze K (1993) Orientation imaging: The emergence of a new microscopy Journal Metallurgical and Materials Transactions A 24:819 – 831

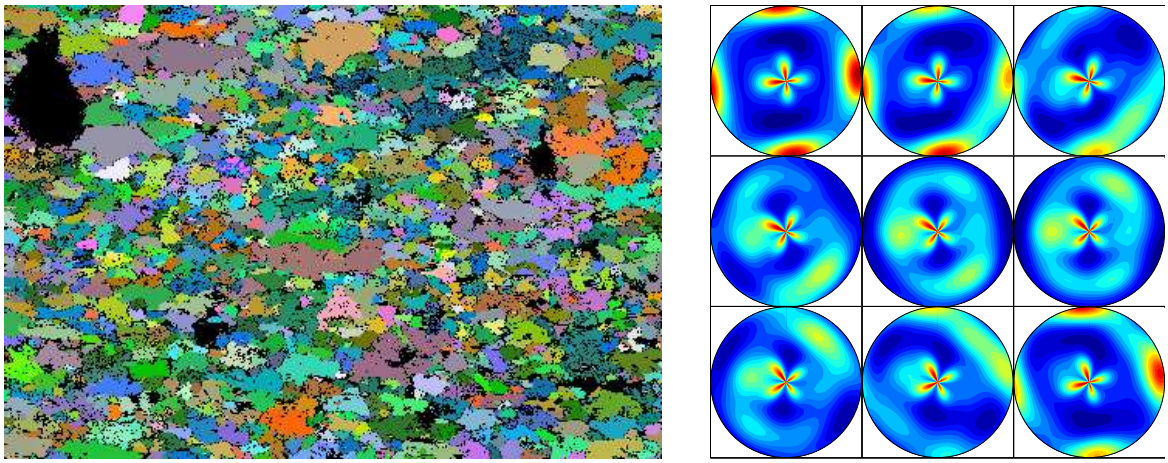

(a) The Raw EBSD data. (b) The estimated ODF.

Figure 7: The plot (a) on the left hand side shows the raw EBSD data. The position within the plot corresponds to the position within the specimen and the RGB values of the colors correspond to the Euler angles of the crystal orientation at this position. The plot (b) on the right hand side shows the estimated ODF $\tilde{f}_{G_M}\colon \mathrm{SO}(3) \to \mathbb{R}$ in sections according to the Euler angles. Red colors indicate high values and blue colors low values.

Askey R (1975) Orthogonal Polynomials and Special functions SIAM, Philadelphia, PA, USA

Berens H, Xu Y (1991) On Bernstein-Durrmeyer polynomials with Jacobi weigts in: Chui CK (editor) Approximation, Interpolation and Functional Analysis Academic Press, Boston pages 25–46

Bochner S (1954) Positive zonale functions on spheres Proc Nat Acad Sci USA

van den Boogaart KG (2001) Statistics for individual crystallographic orientation measurements Ph.D. thesis TU Freiberg

vd Boogaart KG, Hielscher R, Prestin J, Schaeben H (2007) Kernel-based methods for inversion of the radon transform on $\mathrm{SO}(3)$ and their applications to texture analysis J Comput Appl Math 199:122 – 140

Bunge HJ (1982) Texture Analysis in Material Science Butterworths

Fasshauer GE (2007) Meshfree approximation methods with MATLAB World Scientific Publishers

Filbir F, Schmid D (2008) Stability results for approximation by positive definite functions on $SO(3)$ J Approx Theory 153:170 – 183

Frigo M, Johnson SG (2009) FFTW, C subroutine library `http://www.fftw.org`

Gutzmer T (1996) Interpolation by positive definite functions on locally compact groups with application to $SO(3)$ Results Math 29:69–77

Hielscher R (2007) The Radon Transform on the Rotation Group – Inversion and Application to Texture Analysis Dissertation, Department of Mathematics, Technical University Bergakademie Freiberg

Keiner J, Kunis S, Potts D (2006) Fast summation of radial functions on the sphere Computing 78:1 – 15

Keiner J, Kunis S, Potts D (2009a) NFFT 3.0, C subroutine library `http://www.tu-chemnitz.de/~potts/nfft`

Keiner J, Kunis S, Potts D (2009b) Using NFFT3 - a software library for various nonequispaced fast Fourier transforms ACM Trans Math Software 36:Article 19, 1 – 30

Kostelec PJ, Rockmore DN (2006) The SOFT Package: FFTs on the Rotation Group, collection of C routines

Kostelec PJ, Rockmore DN (2008) FFTs on the rotation group J Fourier Anal Appl 14:145 – 179

Kovacs JA, Chacón P, Cong Y, Metwally E, Wriggers W (2003) Fast rotational matching of rigid bodies by fast Fourier transform acceleration of five degrees of freedom Acta Crystallogr Sect D 59:1371 – 1376

Matthies S, Vinel G, Helmig K (1987) Standard Distributions in Texture Analysis volume 1 Akademie-Verlag Berlin

Potts D, Prestin J, Vollrath A (2009) A fast algorithm for nonequispaced Fourier transforms on the rotation group Numer Algorithms 52:355 – 384

Potts D, Steidl G (2003) Fast summation at nonequispaced knots by NFFTs SIAM J Sci Comput 24:2013 – 2037

Varshalovich D, Moskalev A, Khersonskii V (1988) Quantum Theory of Angular Momentum World Scientific Publishing, Singapore

Vilenkin N (1968) Special Functions and the Theory of Group Representations Amer. Math. Soc., Providence, RI, USA

Yershova A, LaValle SM (ICRA 2004) Deterministic sampling methods for spheres and $SO(3)$ in: Proceedings. IEEE International Conference on Robotics and Automation. volume 4 pages 3974 – 3980